Supplementary Information for
"Observation of plaquette fluctuations in the spin-1/2 honeycomb lattice"

Christian Wessler[1][*], Bertrand Roessli[1], Karl W. Krämer[2],
Bernard Delley[1], Oliver Waldmann[3], Lukas Keller[1], Denis
Cheptiakov[1], Hans B. Braun[4,5] & Michel Kenzelmann[1]

[1]Laboratory for Neutron Scattering and Imaging, Paul Scherrer Institut,
Villigen, Switzerland
[2]Department of Chemistry and Biochemistry, University of Bern, Bern,
Switzerland
[3]Physikalisches Institut, Universität Freiburg, Freiburg, Germany
[4]Theoretical Physics, ETH Zürich, Switzerland
[5]Dublin Institute for Advanced Studies, Dublin 4, Ireland
[*]To whom correspondence should be addressed; E-mail:
christian.wessler@psi.ch

Supplementary Note 1. CRYSTAL STRUCTURE

$YbBr_3$ crystallizes with the BiI_3 layer structure in the rhombohedral space group $R\bar{3}$ (148) with lattices parameters of $a = 6.97179(18)$ Å and $c = 19.1037(7)$ Å at room temperature. The lattice parameters are in good agreement with powder[1] and crystal[2] diffraction data found in literature. The unit cell contains six Yb^{3+} ions on site (6c) at (0, 0, z), (0, 0, z) + (2/3, 1/3, 1/3) and (0, 0, z) + (1/3, 2/3, 2/3) with z = 0.1670(2). The Yb ions have C_3 point symmetry and form two-dimensional (2D) honeycomb lattices perpendicular to the c-axis, see Fig. 1. Yb^{3+} has a distorted octahedral coordination by Br^- ions which are located on site (18f) at (x, y, z) with x=0.3331(5), y=0.3131(5), and z=0.08336(15). Surprisingly, the distance between Yb^{3+}-Br^- varies by less than 10^{-2} Å, however the Br^--Yb^{3+}-Br^- bond angles differ significantly between 87.3° and 91.1°. The crystallographic parameters determined on HRPT are summarized in Supplementary Table 1.

Name	x	y	z	occ.
Yb1	0	0	0.33289(21)	0.317(3)
Yb2	0	0	0	0.009(0)
Br	0.35362(57)	0.00022(60)	0.08325(15)	1

Supplementary Table 1: Structural parameters of $YbBr_3$ determined on HRPT at room temperature
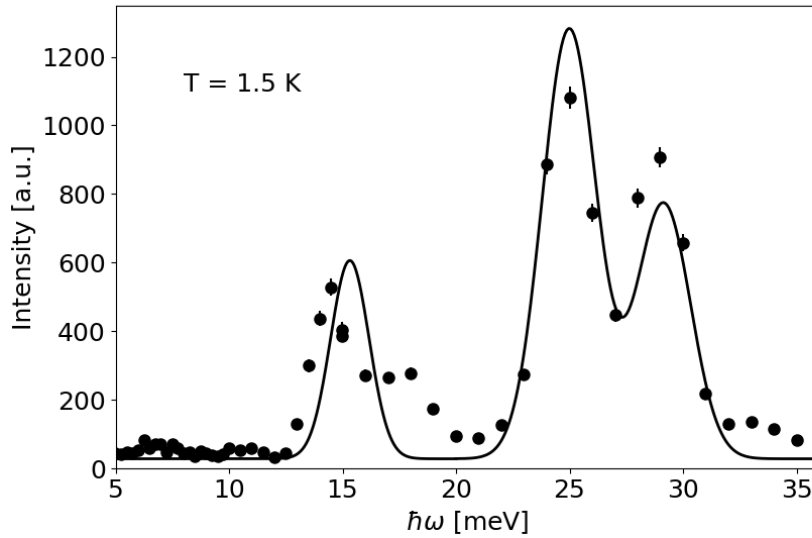
Supplementary Note 2. CRYSTAL ELECTRIC FIELD (CEF)

The electrostatic potential originating from the ions surrounding the Yb^{3+} ion can be modeled with Stevens operators

$$H_{CEF} = \sum_{l,m} B_l^m O_l^m$$

with $B_l^m = \gamma_l^m \theta_l$ and θ_l the Stevens coefficients. For the C_3 point group symmetry of the Yb site only the parameters[3] $B_2^0, B_4^0, B_4^{\pm 3}, B_6^0, B_6^{\pm 3}, B_6^{\pm 6}$ are non-zero. From the inelastic neutron scattering measurement we determined 3 CEF excitations at $E_1 = 14.5$ meV, $E_2 = 25$ meV and $E_3 = 29$ meV. We first used the susceptibility $\chi(T)$ for the determination of the CEF Hamiltonian. From a least-square fit to χ_a and χ_c where a and c denote the crystallographic axis we obtain $\gamma_2^0 = $ -5.14 meV, $\gamma_4^0 = $ -0.59 meV, $\gamma_4^{+3} = 57.43$ meV, $\gamma_4^{-3} = 51.31$ meV, $\gamma_6^0 = 6.09$ meV, $\gamma_6^{+3} = 50.21$ meV, $\gamma_6^{-3} = 55.56$ meV, $\gamma_6^{+6} = 33.9$ meV, $\gamma_6^{-6} = 42.4$ meV. In agreement with the Kramers theorem the CEF splits the $J = 7/2$ multiplet of the Yb^{3+} ion into 4 doublets. The calculated CEF-levels are at 15.16 meV, 24.75 meV, and 28.88 meV, respectively. From a subsequent fit of the inelastic neutron data we obtain very similar values, $\gamma_2^0 = $-6.49 meV, $\gamma_4^0 = $ -0.51 meV, $\gamma_4^{+3} = $58.53 meV, $\gamma_4^{-3} = $52.12 meV, $\gamma_6^0 = 6.01$ meV, $\gamma_6^{+3} = 48.11$ meV, $\gamma_6^{-3} = 56.30$ meV, $\gamma_6^{+6} = 33.21$ meV, $\gamma_6^{-6} = 41.12$ meV. We show in Supplementary Fig. 1 a comparison between calculated and observed neutron scattering intensities. We point out that the first excited CEF-level has a double-peak structure in $YbBr_3$ that is not explained by our model. It also resembles the CEF levels[4] of $YbCl_3$ and

thus this issue requires further investigation. Nevertheless the CEF-model presented here provides an adequate description of the temperature dependence of the static susceptibility. In addition we performed a point charge calculation based on the program multiX.[5] In agreement with the susceptibility measurements, calculations show that at high temperatures anisotropy is small in YbBr$_3$ with easy-plane anisotropy developing below $T = 50$ K. At $T = 4$ K, we obtain $\chi_a \approx 1.3\chi_c$.

Supplementary Fig. 1 | Yb^{3+} crystal electric field in YbBr$_3$. Crystal electric field (CEF) excitations measured by inelastic neutron scattering. The solid line is the calculated intensity. Error bars are standard deviations.

4

Supplementary Note 3. MAGNETIC EXCITATIONS

Because of the large separation between the ground-state and the first CEF doublet, the magnetic properties of $YbBr_3$ can be approximated by a spin $S = 1/2$. Choosing a local coordinate frame with the ζ-axis oriented along a given spin direction, the non-zero elements of the single-ion susceptibility matrix are $\chi_0^{\xi\xi}(\omega) = \chi_0^{\eta\eta}(\omega)$ and $\chi_0^{\xi\eta}(\omega) = -\chi_0^{\eta\xi}(\omega)$ which correspond to excitations transverse to the (local) spin direction. Within mean-field approximation,

$$\chi_0^{\xi\xi}(\omega) = \frac{1}{2}\frac{\Delta}{\Delta^2 - (\omega + i\epsilon)^2} \tag{1}$$

$$\chi_0^{\xi\eta}(\omega) = \frac{i}{2}\frac{\omega + i\epsilon}{\Delta^2 - (\omega + i\epsilon)^2}, \tag{2}$$

with $\Delta \equiv \Delta_i = -\langle S_\zeta \rangle \sum_j \mathcal{J}_{\zeta\zeta}(i,j)$ the local field acting on a given Yb moment with $\mathcal{J}$ defined in Eq. (1) and ϵ the finite line width of the excitations. Within linear spin-wave theory, the dipole-dipole interactions induce a gap in the spin-wave dispersion.[9, 10] With a Yb magnetic moment of 2 μ_B, the dipolar interactions produce a spin gap at the zone center ~ 200 μeV. The easy-plane anisotropy favors alignment of the spins in the hexagonal plane. The spin gap opened by H_{dip} is reduced by the easy-plane anisotropy. At $g_{crit} \sim 0.985$ the spin gap is minimal and below that value the spins rotate into the basal plane, see Supplementary Fig. 2. The easy-plane anisotropy lifts the degeneracy of the spin wave branches at the zone center and the splitting increases with increasing anisotropy.
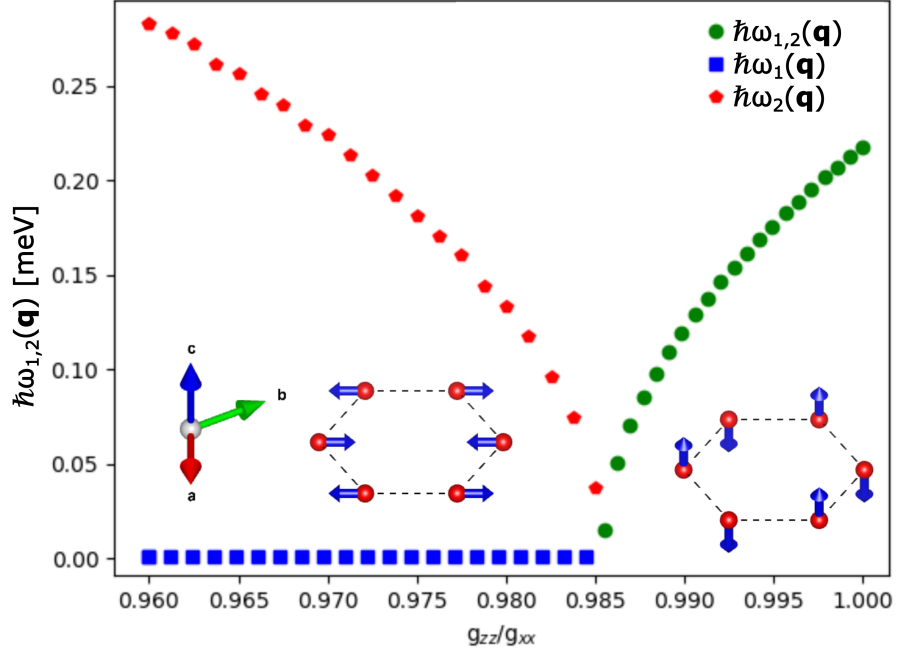
Supplementary Fig. 2 | Dependence of the energy gap as a function of easy-plane anisotropy. Above $g_{zz}/g_{xx} = 0.985 = g_{crit}$, the calculated branches $\omega_1(q)$ and $\omega_2(q)$ are degenerate while for $g_{zz}/g_{xx} < g_{crit}$ the two spin-wave branches split. All points are calculated with a precision of $\sim$ 0.005 meV. The magnetic configurations shown in the figure correspond to a Néel antiferromagnet with spins aligned along the c-axis for $g_{zz}/g_{xx} > 0.985$ and in the hexagonal plane for $g_{zz}/g_{xx} < 0.985$.

We have also simulated the two-magnon scattering expected for a Heisenberg Hamiltonian[11] as shown in Supplementary Fig. 3. for the the (1,0,0) Brlllouin zone. Our calculations show a broad continuum extending up to twice the maximum of the spin wave excitations. In contrast to our observations, the two-magnon continuum is present in the complete Brillouin zone and is strongest close to the zone center.

6
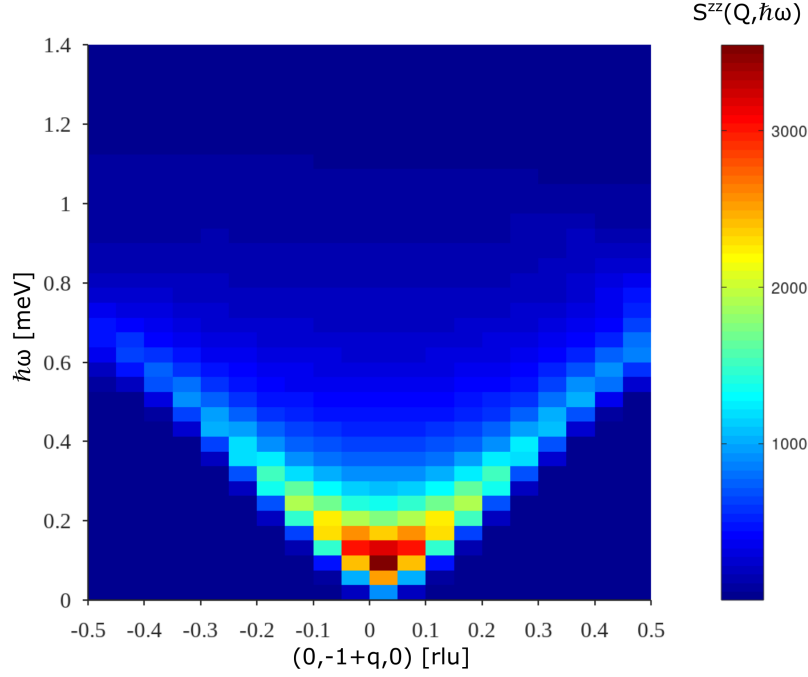
Supplementary Fig. 3 | Calculated two-magnon cross-section for a Heisenberg Hamiltonian. An arbitrary cutoff is introduced in the dispersion of the spin-waves to avoid divergence of the two-magnon cross-section at the zone center.

Supplementary Note 4. MAGNETIC GROUND-STATE

In mean field theory, the classical ground-state is given by the eigenvectors of the largest eigenvalue $\lambda\,(\mathbf{q})$ of the Fourier transform of the interaction matrix $\overline{\overline{M}}(\mathbf{q})$.[6–8] Based on the Hamiltonian $H_{\mathrm{h}} + H_{\mathrm{dip}}$, $\lambda\,(\mathbf{q})$ has a maximum at $\mathbf{Q}_0 = (0,0,0)$ which agrees with the diffuse scattering observed in $YbBr_3$ (see Fig. 2a). We find that the dipolar energy becomes independent of the distance between the Yb-planes for a lattice parameter $c > 12$ Å, which

shows that the 2D limit is reached in $YbBr_3$ and inter-layer interactions can be neglected.

Supplementary Note 5. MAGNETIC SUSCEPTIBILITY

The temperature dependence of the static susceptibility χ is shown in Fig. 1c for magnetic field orientations in-plane (a-axis) and out-of-plane (c-axis). χT values (not shown) increase with temperature and do not saturate up to 300 K. The values at 300 K are 2.282 and 2.687 cm^3K/mol along the a- and c-axes, respectively. The average of 2.417 cm^3K/mol is slightly below the expectation value of 2.572 cm^3K/mol for the $^2F_{7/2}$ ground-state of Yb^{3+}. At lower temperature a maximum in the χ versus T curves is observed at $T = 2.75$ K. We have calculated the temperature dependence of the static susceptibility for an Yb_6 honeycomb with the exchange parameters determined from the spin-wave analysis and easy-plane anisotropy parameters $g_a/g_c = 1.25$. We find that the susceptibility has a broad maximum around $T \simeq 4$ K and reproduces the experimental χ (T) above 5 K well, as shown in Supplementary Fig. 4.
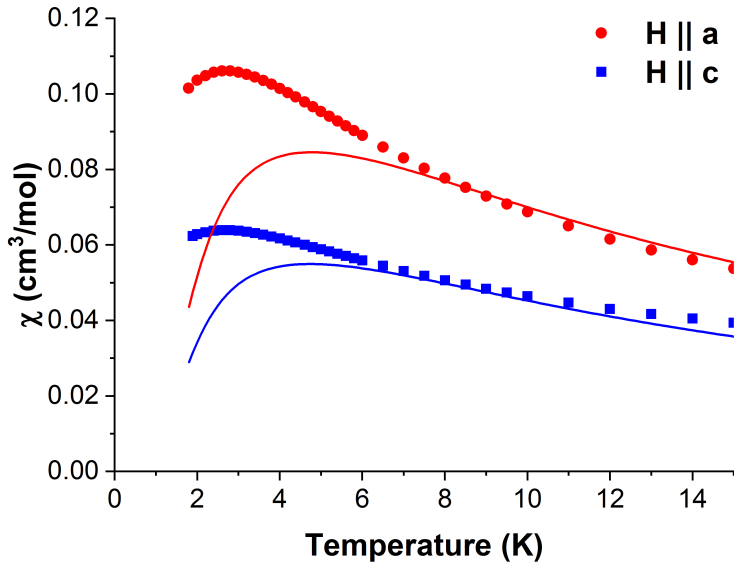
Supplementary Fig. 4 | Calculated susceptibility for a Yb$_6$ hexamer. The measured low-temperature magnetic susceptibility is shown together with the calculation (solid lines) for a single plaquette with $S = 1/2$, and the Hamiltonian $H_\mathrm{h} + H_\mathrm{dip}$ of the main text. Error bars are standard deviations.

Supplementary References

1. Meyer, G. Private communication to powder diffraction data base (PDF2), no. [42-0968] (1990).

2. Brenner, M. Kinetische Studien zu Phasenumwandlungen zwischen polymorphen Formen von $YbBr_2$ sowie die Bestimmung der Kristallstruktur von $YbBr_3$. Dissertation Universität Karlsruhe (1997).

3. Bauer, E. & Rotter, M. Magnetism of complex metallic alloys: crystalline electric field effects. in *Series on Complex Metallic Alloys* Vol. 2, ed. E. Belin-Ferr, World Scientific (2009).

4. Sala, G. *et al.* Crystal field splitting local anisotropy, and low-energy excitations in the quantum magnet $YbCl_3$. *Phys. Rev.* B **100**, 180406(R) (2019).

5. Uldry, A., Vernay, F. & Delley, B. Systematic computation of crystal-field multiplets for x-ray core spectroscopies. *Phys. Rev. B* **85**, 125133 (2012).

6. Reimers, J.N. Diffuse-magnetic-scattering calculations for frustrated antiferromagnets. *Phys. Rev. B* **46**, 193-202 (1992).

7. Kadowaki, H., Ishii, Y., Matsuhira, K. & Hinatsu, Y. Neutron scattering study of dipolar spin ice $Ho_2Sn_2O_7$: Frustrated pyrochlore magnet. *Phys. Rev. B* **65**, 144421 (2002).

8. Enjalran, M. & Gingras, M.J.P. Theory of paramagnetic scattering in highly frustrated magnets with long-range dipole-dipole interactions: The case of the $Tb_2Ti_2O_7$ pyrochlore antiferromagnet. *Phys. Rev. B* **70**, 174426 (2004).

9. Pich, C. & Schwabl, F. Order of two-dimensional isotropic dipolar antiferromagnets. *Phys. Rev.* B **47**, 7957-7960 (1993).

10. Pich, C. & Schwabl, F. Spin-wave dynamics of two-dimensional isotropic dipolar honeycomb antiferromagnets. *JMMM* **148**, 30-31 (1995).

11. Heilmann, I.U. *et al.* One- and two-magnon excitations in one-dimensional antiferromagnet in a magnetic field. *Phys. Rev. B* **24**, 3939-3953 (1981).